# Optical Generation and Transmission of mmWave Signals in 5G ERA: Experimental Evaluation Paradigm

Efstathios Andrianopoulos, Nikolaos K. Lyras, *Member, IEEE*, Christos Tsokos, Tianwen Qian, Simon Nellen, David de Felipe, Panos Groumas, Adam Raptakis, Lefteris Gounaridis, Norbert Keil, Christos Kouloumentas, and Hercules Avramopoulos, *Member, IEEE*

***Abstract*— We demonstrate the generation, of a mmWave signal via the injection of an optical frequency comb (OFC) into an integrated tunable dual distributed Bragg reflector (DBR) laser as well as the fiber transmission and the processing of this signal by an optical beamforming network (OBFN). The dual DBR laser is based on a hybrid indium phosphide (InP) – polymer photonic integrated circuit (PIC). Two different cases have been examined in which the microwave signal is centered around 39 GHz and 60 GHz respectively, carrying quadrature amplitude modulation (QAM) formats at 0.5 Gbaud. In this proof-of-concept scenario, the OBFN consists of two optical paths, where the relative true time delay is induced by an optical delay line (ODL). Extensive comparison between the back-to-back (B2B) case and scenarios with transmission over 25 km of standard single-mode fiber (SSMF) has been made using the error-vector magnitude (EVM) and the bit-error ratio (BER) as evaluation criteria. In all cases, error-free transmission was suggested for all QPSK signals, whereas a worst-case EVM of 11.8% was observed for 16-QAM transmission, successfully showcasing the concept's potential. The generated microwave signal's frequency can be set arbitrarily high, provided that high-speed photodetection equipment is available for the detection and down-conversion of the signal. Extension to higher antenna elements (AEs) numbers is straight-forward, relying only on the number of available photodetectors.**

***Index Terms*— Microwave photonics, optical beamforming network, injection locking, fiber transmission, photonic integrated circuits, millimeter wave technology, terahertz communications.**

Manuscript received 22 June 2022; revised 21 July 2022; accepted 27 July 2022. Date of publication 10 August 2022; date of current version 22 August 2022. This work was supported by the European Horizon 2020 Project Information and Communication Technologies (ICT)-TERAWAY, Research and Innovation (R&I) Programme, Initiative of Photonics Public Private Partnership (PPP), under Grant 871668. *(Corresponding author: Efstathios Andrianopoulos.)*

Efstathios Andrianopoulos, Nikolaos K. Lyras, Adam Raptakis, Lefteris Gounaridis, and Hercules Avramopoulos are with the Photonic Communications Research Laboratory, National Technical University of Athens, Zografou, 15573 Athens, Greece (e-mail: efand@mail.ntua.gr).

Christos Tsokos is with LioniX International BV, 7500 AL Enschede, The Netherlands (e-mail: c.tsokos@lionix-int.com).

Tianwen Qian, Simon Nellen, David de Felipe, and Norbert Keil are with the Fraunhofer Institute for Telecommunications, Heinrich-Hertz-Institut, 10587 Berlin, Germany (e-mail: tianwen.qian@hhi.fraunhofer.de).

Panos Groumas and Christos Kouloumentas are with the Photonic Communications Research Laboratory, National Technical University of Athens, Zografou, 15573 Athens, Greece, and also with Optagon Photonics, Agia Paraskevi, 15341 Athens, Greece (e-mail: christos.kouloumentas@optagon-photonics.eu).

Color versions of one or more figures in this letter are available at https://doi.org/10.1109/LPT.2022.3196632.

Digital Object Identifier 10.1109/LPT.2022.3196632

## I. Introduction

THE emerging applications enabled by the deployment of the fifth generation (5G) of cellular networks and beyond, increase the demand for higher data rates. Thus, utilization of higher frequency bands in the mmWave regime, where larger spans of unallocated spectrum are available becomes essential. To that end, significant reduction of the cell size is required, thus increasing the number of cells that need to be deployed to provide sufficient coverage. To minimize the cost and increase the spectral efficiency of the 5G picocellular system, a centralized approach for the generation of the mmWave signals, together with analog radio over fiber (A-RoF) techniques for the distribution network emerges as a promising solution [1].

Furthermore, significant increase in the number of the wireless base stations (BS) is expected, aiming to accommodate the rapid growth of mobile data traffic. For this reason, beamforming techniques emerge as a necessity, due to their ability to generate highly directive beams, and thus compensate for the high free-space path losses and prevent the radio interference between adjacent BSs. Optical beamforming techniques are an attractive approach offering electromagnetic interference immunity, frequency transparency, and reduced weight, size and power consumption [2].

To overcome the limitations imposed by the phase noise in the optical generation of mmWave signals with heterodyning techniques, A-RoF scenarios enabled by phase locking schemes have been extensively studied, using among others optical frequency comb generation, self-homodyning, and sideband-locking techniques [1], [3]–[5]. Dual wavelength fiber lasers have also been gaining attention due to their ability to provide coherent and tunable optical sources [6]. Moreover, optical beamforming solutions combined with A-RoF transmission have been investigated implementing photonic integrated array-antennas [7] and multi-beamforming scenarios [8]. However, in these scenarios no phase locking scheme was used, imposing limitations on the generated microwave carrier. To our knowledge, no work has showcased the possibility to combine the aforementioned techniques, offering a complete solution for the generation, distribution and emission of mmWave signals in a central station to remote BS interconnection scenario.

In this work we experimentally demonstrate the generation of mmWave signals with central frequencies around 39 GHz and 60 GHz respectively, which have been identified as key

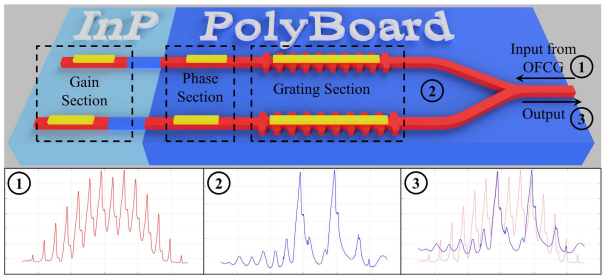


Fig. 1. Layout of the dual DBR laser. Insets: Spectra: 1) OFC, 2) Dual laser's output (free-running), 3) Previous two superimposed.

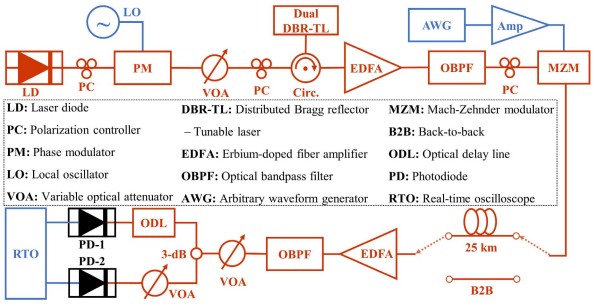


Fig. 2. Schematic layout of the experimental setup.

frequency bands within the 5G network framework [9], carrying QPSK and 16-QAM modulation formats at 0.5 Gbaud. This is enabled by injecting an optical frequency comb (OFC) into a state-of-the-art dual tunable DBR laser. This all-optical technique for mmWave signal generation, straight-forwardly enables the introduction of optical beamforming solutions, as well as optical distribution through an A-RoF scheme. After a 25 km transmission through an SSMF, the signal is being processed by a $1 \times 2$ optical beamforming network (OBFN). The evaluation of our setup is realized by means of error-vector magnitude (EVM) and bit-error ratio (BER) measurements of the decoded signals at the intended beam angles. Generation of multiple independent mmWave tones is feasible on-chip, provided that more tunable laser sources are integrated. The frequency of the generated microwave signal can be set arbitrarily high, provided that high-speed photodetectors are available, able to detect the optical beat signal. Furthermore, extension to larger scale OBFN is straight-forward, relying only on the number of available photodetectors and ODLs.

## II. Experimental Setup

A key building block of our setup is a cutting edge dual DBR laser leveraging the hybrid integration of InP and polymer in the PolyBoard platform, which offers cost efficiency and significant performance advantages in terms of, among others tuning efficiency, reliability and output power [10]. A schematic representation of the PIC is depicted in Figure 1. More specifically, the laser provides two independently tunable optical laser lines with 18 nm wavelength tuning range each, enabled by the grating section (coarse tuning) and the phase section (fine tuning). The tuning efficiency and stability of the laser permit us to phase lock the two tones, and as a result generate high purity RF signals, limited frequency-wise only by the bandwidth of the photodetection process. Injection locking techniques employing multiple architectures have been also successfully demonstrated in [11]–[13].

Figure 2 depicts the experimental setup for the evaluation of the proposed architecture consisting of the injection locking, fiber transmission and optical beamforming stages. A tunable laser diode (Santec WSL-110) serves as the optical input of the OFC generation (OFCG) unit. The optical modulation element of the OFCG unit is implemented via a 40-GHz phase modulator (Thorlabs LN66S-FC, PM), paired with a polarization controller (PC). An RF local oscillator (Anritsu MG3694B, LO) provides the electrical input to the PM. At the output of the OFCG unit, an optical circulator is responsible for the injection of the OFC into the dual DBR laser, and guiding the resulting optical signal with the phase-locked carriers to the optical chain's next stage. A variable optical attenuator (VOA) along with a second PC are also used to control the power and polarization state of the OFC, optimizing the injection locking process. The generated OFC tones are equidistant, with frequency distance equal to the LO's frequency.

As shown in the insets of Figure 1, the phase locking is achieved by carefully tuning the output wavelengths of the two tones of the laser PIC to coincide with the desired tones of the OFC. In our case, the 1$^{st}$ order fundamentals of the OFC were used for the locking process, maximizing their power by tuning the RF power provided by the LO. The injection ratio [13] was equal to $-32$ dB, providing a frequency detuning range of 360 MHz. The tuning of the laser's power and wavelength was enabled by a high-precision current source (ILX Lightwave LDC-3916) that was used to drive the lasers' different sections, as well as a thermo-electric controller for temperature stability.

At the output of the injection locking process, an erbium-doped fiber amplifier (EDFA) along with an optical bandpass filter (OBPF) are used to amplify the optical signal and filter out the out-band noise. Another PC is used to optimize the modulation process, which is realized by a 40-Gb/s Mach-Zehnder modulator (Fujitsu FTM7937EZ, MZM). At the electrical input of the MZM, a 65 GSa/s arbitrary waveform generator (Keysight M8195A, AWG) coupled with an RF amplifier (SHF S126A), produces QPSK and 16-QAM microwave signals around a 1.5 GHz microwave carrier, with 0.5 Gbaud symbol rate. Using a raised cosine pulse shaping filter with a roll-off factor equal to 1, the spectral content of the signals is confined in a 1 GHz bandwidth around their carrier.

After the modulation stage, either directly (back-to-back case) or after a 25 km transmission through an SSMF, the signal enters a second amplification stage consisting of an EDFA and OBPF pair, coupled with a VOA, before reaching the optical beamforming stage. In this proof-of-concept scenario, the OBFN consists of two AEs, where two high-speed PDs with 3-dB bandwidths equal to 50 and 70 GHz (II-VI XPDV2320R and XPDV3120R, PD-1, and $-2$ respectively in Figure 2) were used. Therefore, a VOA was implemented in the path of PD-2 to compensate for the different frequency responses of the PDs, equalizing the power of the two signals after the photodetection stage.

After photodetection, the signals are sampled and stored by a real-time oscilloscope (Keysight UXR0704AP, RTO) with 70 GHz analog bandwidth and 256 GSa/s sampling rate. To limit the impact of the noise accommodated by the oscilloscope, and taking into account that the noise power is dictated by the measuring bandwidth, a bandwidth limit

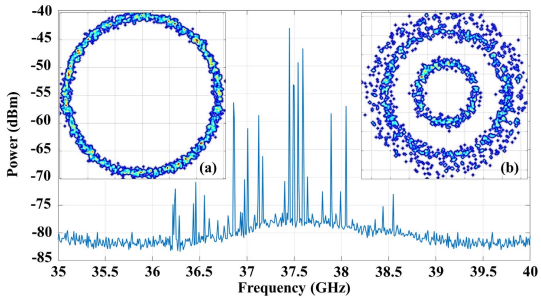


Fig. 3. Generated microwave tone spectrum in free-running mode. Insets: Indicative constellations:(a) QPSK, (b) 16-QAM signals.

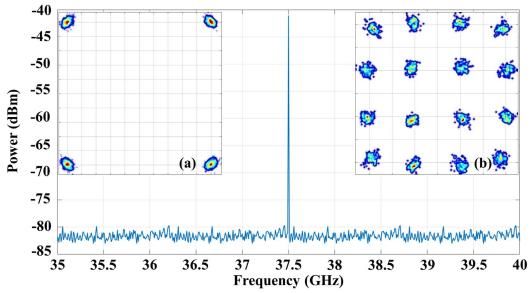


Fig. 4. Generated microwave tone spectrum in injection-locked mode. Insets: Indicative constellations:(a) QPSK, (b) 16-QAM signals.

was set at the oscilloscope, adapted to each experimental scenario. In total, 5.120.000 samples are acquired from the RTO for offline processing, which includes the calculation of the radiated field assuming transmission through a phased array antenna, detection by a single omnidirectional AE at the receiver side placed at the nominal transmission angle, down conversion of the detected microwave signal to the baseband, and extraction of the in-phase and quadrature (I/Q) components whilst filtering out the unwanted spectral content by means of a low-pass filtering unit. Finally, a standard set of digital signal processing (DSP) algorithms is used comprising an amplitude level correction unit, a time recovery unit, a dispersion compensation unit, a time-domain equalization unit and a carrier phase recovery unit, before extracting the final EVM and BER values.

## III. Experimental Results

Figures 3 and 4 depict the spectrum of the microwave carrier that is generated after the photodetection stage, as a result of the beating of the two optical carriers from the dual DBR laser in free-running operation and in locked operation, respectively. The spectra showcase the generated carrier within a 5 GHz span around its nominal value, acquired with 30 kHz resolution bandwidth. In both figures' insets, two indicative constellation diagrams of QPSK and 16-QAM signals are shown, for the reported operations. Specifically, these insets depict 0.5 Gbaud QPSK/16-QAM signals generated around an intermediate frequency (IF) of 1.5 GHz, that were generated, stored, and processed through the developed DSP suite.

As can be observed, in the free-running operation, the generated microwave carrier suffers from significant phase noise that strongly deteriorates its quality. In the scenario where the optical carriers are modulated with a microwave signal before the photodetection stage, this phase noise is

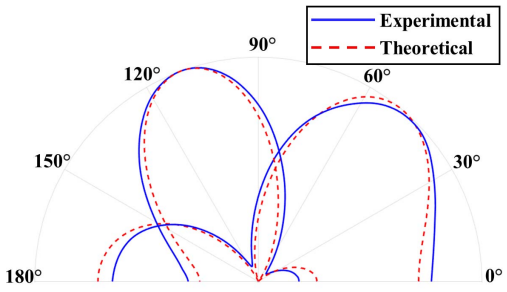


Fig. 5. Comparison of the emulated radiation patterns the experimental and theoretical results for angles 50° and 110°.

evident, and translates to the tangent noise that exists in both the QPSK and 16-QAM constellation diagrams.

In contrast, when the optical carriers are locked via the injection locking process, their phase noises become correlated and are suppressed during the photodetection stage. As a result, the generated microwave carrier has almost negligible phase noise as can be observed in Figure 4. The tangent noise of the respective constellations diagrams is eliminated in this case, providing significantly higher signal quality after the demodulation stage. The amplitude noise that exists in both cases is due to the Gaussian noise generated by the two EDFAs. The beamforming capabilities of our setup are evaluated by emulating a wireless system operating in the downlink direction, where the microwave signals are emitted by a 2-element $\lambda/2$-spaced antenna array. Figure 5 depicts two sequential measurements of the time averaged radiations extracted by the samples acquired from the oscilloscope, when the system transmits quadrature modulated signals, assuming omnidirectional antenna elements. Two cases are shown, where our system transmits beams directed at 110° carrying a 0.5 Gbaud QPSK signal at 39 GHz central frequency, and at 50° carrying a 16-QAM signal at 60 GHz, respectively. The red dashed line represents the theoretical value of the array factors, for the intended beam angles. As observed, the theoretical and the experimental values agree in principle. The pointing deviation observed in the second case (beam directed at 50°) is mainly caused by the resolution of the ODLs since, when the spacing between the AEs is proportional to the wavelength of the signal ($\lambda/2$ in our case), the delay amount necessary for beam steering is inherently inversely proportional to the frequency of the signal [14]. Thus, any slight mismatch between the desired and the imposed delay causes more evident deviation in the 60 GHz case, and almost non-existent in the lower transmission frequency case.

Finally, we evaluate the operation of the complete system, as described in Section II. More specifically, we evaluate the performance of our setup, using the corresponding EVM value as the mean of evaluation, with respect to the received optical power incident to the photodiodes, in eight different scenarios defined by the modulation format, the central microwave frequency and the existence of fiber transmission. In each scenario, three different beam angles are examined, i.e., 50°, 90° and 110°. Figures 6(a), (b) depict the EVM measurements of the 39 GHz microwave signal, for B2B configuration and after 25 km SSMF transmission respectively, as a function of the received optical power (ROP) before the photodetection

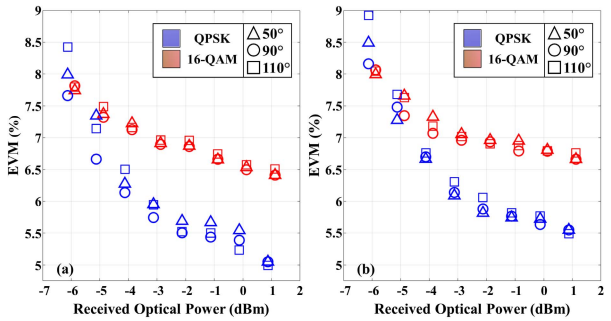


Fig. 6. EVM w.r.t the received optical power for the 39 GHz mmW signal, (a) in B2B configuration and (b) after 25 km fiber transmission.

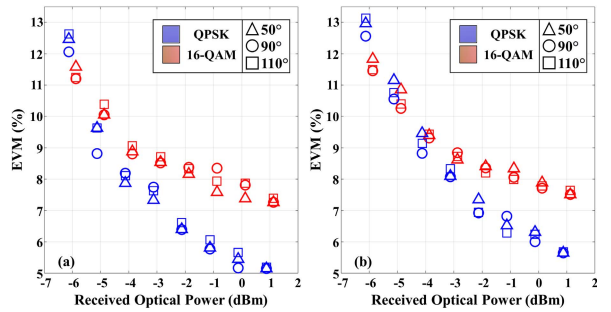


Fig. 7. EVM w.r.t the received optical power for the 60 GHz mmW signal, (a) in B2B configuration and (b) after 25 km fiber transmission.

stage. As expected, for higher values of the ROP, the 16-QAM signal exhibits higher values of EVM compared to the QPSK, increasing however with a smaller slope as the ROP decreases, and ultimately converging to a smaller value. This result is reasonable to observe, considering the inherent form of the constellation diagrams of each modulation format.

The slight EVM deviation observed between the targeted angles stems from the Gaussian noise accommodated in the signal. This deviation is rationally more evident for smaller ROP values, where the noise power density of the oscilloscope is more impactful. The same applies in Figure 7 where the EVM curves for the 60 GHz signal are depicted. The EVM values begin at around the same values as in the 39 GHz case, but increase with a higher rate as the ROP decreases, reaching significantly higher values in the low ROP regime. This can be explained considering that, since the frequency of the microwave signal is higher, the measurement bandwidth of the oscilloscope was also increased as explained in Section II, rendering the oscilloscope's noise more impactful. Adding to this, higher amplification was necessary to compensate for the power imbalance in the path of PD-1, since the microwave signal was centered around a higher frequency than its 3-dB bandwidth, lowering the path's overall SNR. However, single-digit EVM values are obtained for all measurements corresponding to the 39 GHz case, translating to a worst-case scenario BER equal to $7.48 \cdot 10^{-6}$ for the 16-QAM signals, whereas the corresponding worst-case scenario for the 60 GHz 16-QAM signals resulted in BER equal to $1.8 \cdot 10^{-3}$. Error-free transmission was feasible for all QPSK signals.

## IV. Conclusion

In this work an all-optical system for the generation, transmission, and processing through an OBFN of mmWave signals is studied, taking advantage of photonic techniques. The setup is enabled by the injection locking process, where an OFC is injected into a dual-DBR laser PIC, phase-locking the two optical sources at its output. Two mmWave frequencies were examined, namely 39 and 60 GHz, identified as key frequency bands within 5G network frameworks. After having verified the system's potential to produce mmW tones with minimal phase noise, we evaluated its EVM performance using QPSK and 16-QAM signals at 0.5 Gbaud symbol rate, for different target angles, under B2B and 25 km fiber transmission scenarios. Error-free transmission was feasible for all QPSK signals, whereas for the 16-QAM signals, a worst-case EVM of 8.1% and 11.8% was observed for the 39 GHz and 60 GHz case respectively. Scaling to a larger OBFN is straightforward, provided that a higher number of ODLs and PDs is available.

## References

[1] R. P. Braun, G. Grosskopf, D. Rohde, and F. Schmidt, "Low-phase-noise millimeter-wave generation at 64 GHz and data transmission using optical sideband injection locking," *IEEE Photon. Technol. Lett.*, vol. 10, no. 5, pp. 728–730, May 1998, doi: 10.1109/68.669405.

[2] C. Tsokos *et al.*, "True time delay optical beamforming network based on hybrid InP-silicon nitride integration," *J. Lightw. Technol.*, vol. 39, no. 18, pp. 5845–5854, Sep. 1, 2021, doi: 10.1109/JLT.2021.3089881.

[3] P. D. Lakshmijayasimha *et al.*, "A novel mmW A-RoF transmission scheme employing dual-stage active demultiplexing of an optical frequency comb," in *Proc. ECOC*, Dec. 2020, pp. 1–4, doi: 10.1109/ECOC48923.2020.9333254.

[4] S. T. A., P. D. Lakshmijayasimha, C. Browning, P. M. Anandarajah, L. P. Barry, and A. Kaszubowska-Anandarajah, "Optical frequency comb and active demultiplexer-enabled 60 GHz mmW ARoF transmission using directly modulated 64-QAM UF-OFDM signals," in *Proc. Conf. Lasers Electro-Optics Eur. Quantum Electron. Conf. (CLEO/Europe-EQEC)*, Jun. 2021, p. 1.

[5] A. H. M. R. Islam, M. Bakaul, A. Nirmalathas, and G. E. Town, "Millimeter-wave radio-over-fiber system based on heterodyned unlocked light sources and self-homodyned RF receiver," *IEEE Photon. Technol. Lett.*, vol. 23, no. 8, pp. 459–461, Apr. 1, 2011, doi: 10.1109/LPT.2011.2107894.

[6] S. E. Alavi, M. R. K. Soltanian, I. S. Amiri, M. Khalily, A. S. M. Supa'at, and H. Ahmad, "Towards 5G: A photonic based millimeter wave signal generation for applying in 5G access fronthaul," *Sci. Rep.*, vol. 6, no. 1, pp. 1–11, Apr. 2016.

[7] K. Furuya, T. Hirasawa, M. Oishi, S. Akiba, J. Hirokawa, and M. Ando, "60 GHz-band photonic-integrated array-antenna and module for radio-over-fiber-based beam forming," *IEICE Trans. Commun.*, vol. 100, no. 10, pp. 1717–1725, 2017, doi: 10.1587/transcom.2017OBI0001.

[8] X. Ye, F. Zhang, and S. Pan, "Optical true time delay unit for multi-beamforming," *Opt. Exp.*, vol. 23, no. 8, p. 10002, Apr. 2015, doi: 10.1364/OE.23.010002.

[9] X. Wang *et al.*, "Millimeter wave communication: A comprehensive survey," *IEEE Commun. Surveys Tuts.*, vol. 20, no. 3, pp. 1616–1653, Jun. 2018, doi: 10.1109/COMST.2018.2844322.

[10] D. de Felipe *et al.*, "Polymer-based external cavity lasers: Tuning efficiency, reliability, and polarization diversity," *IEEE Photon. Technol. Lett.*, vol. 26, no. 14, pp. 1391–1394, Jul. 2014.

[11] G. Carpintero, S. Hisatake, D. de Felipe, R. Guzman, T. Nagatsuma, and N. Keil, "Wireless data transmission at terahertz carrier waves generated from a hybrid InP-polymer dual tunable DBR laser photonic integrated circuit," *Sci. Rep.*, vol. 8, no. 1, pp. 1–7, Dec. 2018, doi: 10.1038/s41598-018-21391-0.

[12] L. Gonzalez-Guerrero *et al.*, "Injection locking properties of an InP-$Si_3N_4$ dual laser source for mm-wave communications," *J. Lightw. Technol.*, early access, May 11, 2022, doi: 10.1109/JLT.2022.3171080.

[13] Z. Liu and R. Slavik, "Optical injection locking: From principle to applications," *J. Lightw. Technol.*, vol. 38, no. 1, pp. 43–59, Jan. 1, 2020.

[14] R. Mailloux, *Phased Array Antenna Handbook*. Norwood, MA, USA: Artech House, 2005.